Chemical Science

ROYAL SOCIETY OF CHEMISTRY

EDGE ARTICLE

View Article Online
View Journal | View Issue

Check for updates

Cite this: *Chem. Sci.*, 2025, **16**, 23203

All publication charges for this article have been paid for by the Royal Society of Chemistry

Received 20th August 2025
Accepted 25th October 2025

DOI: 10.1039/d5sc06353a

rsc.li/chemical-science

Open Access Article. Published on 27 October 2025. Downloaded on 2/6/2026 11:08:24 AM. This article is licensed under a Creative Commons Attribution-NonCommercial 3.0 Unported Licence.

DMF/DMSO-catalyzed selective ring-opening polymerization of salicylate cyclic esters

Ge Yao,[a] Jiyu Liu,[a] Hongjun Fu,[a] Chunmei Wang,[a] Guojie Li,[a] Luya Cao,[b] Xiaobo Pan[a] and Jincai Wu *[a]

Salicylate copolyesters are promising biomedical materials due to their biodegradability, biocompatibility, and bioactivity. Eliminating toxic catalyst/initiator residues in polymers is of great importance for their medical applications; however, achieving this remains a formidable challenge in controllable high-molecular-weight polyester synthesis in certain cases. In this work, dimethylformamide (DMF) and dimethyl sulfoxide (DMSO) as weak hydrogen-bonding catalysts are found to efficiently catalyze the controllable ring-opening polymerization (ROP) of salicylate cyclic esters, where the phenolic ester bond in the monomer is selectively cleaved rather than that in the polymer chains. Therefore, high-molecular-weight salicylate copolyesters in a controlled manner ($M_{n,\ PSG}$ = 177.5 kg mol^{-1} and $M_{n,\ PSMG}$ = 530.0 kg mol^{-1}) are successfully synthesized due to effective suppression of backbiting and intermolecular transesterification side reactions. DMF and DMSO are easily removed through devolatilization after polymerization, eliminating tedious purification steps and toxicity concerns for potential medical applications. In addition, the polymerization remains well-controlled even in the presence of water. Theoretical calculations indicate that DMF/DMSO catalyze the ROP through weak hydrogen interactions with the monomer and initiator/phenolic propagation species, which enables the selective ROP of salicylate cyclic esters.

Introduction

The production of biodegradable polymers reached 2.47 million tonnes in 2024 and will hit 5.73 million tonnes by 2029 (ref. 1) due to their potential to end plastic pollution.[2,3] Among them, polyesters such as polylactide (PLA), polycaprolactone (PCL), poly(glycolic acid) (PGA), poly(hydroxy alkanoates), and poly(butylene adipate-*co*-terephthalate) are the primary ones.[4–13] Some of them are widely applied in the drug, food, and healthcare industries due to their good biocompatibility. For medical applications, catalyst residues in polymers are subject to strict limits; for example, tin residues in medical-grade polylactide are required to be below 20 ppm by the U.S. Food and Drug Administration (FDA).[14,15] Therefore, non-toxic metal and metal-free catalysts are widely explored.[16–28] However, the toxicity of organic catalysts and most ligands of non-toxic metal complexes remains ambiguous.

Salicylate-based polyesters are promising medical polymers that exhibit better biodegradability than polylactide.[4,29,30] In addition, salicylate-based copolyesters can demonstrate good antimicrobial activity.[31] However, the synthesis methodology for high-molecular-weight salicylate-based polyesters still requires further exploration because the highly active phenolic ester bonds in monomer and polymer chains lead to serious side reactions during the ROP of related cyclic esters, such as intermolecular transesterification and backbiting reactions when using tin(II) 2-ethylhexanoate ($Sn(Oct)_2$)[30] or 4-dimethylaminopyridine (DMAP)[32] as a catalyst. Therefore, synthesizing high-molecular-weight salicylate-based polyesters is challenging. Recently, it was reported that tetrabutylammonium halides can selectively ring-open monomers while remaining inactive toward polymer chains in bulk polymerization, and high-molecular-weight lactic acid salicylate copolyester (PSMG with M_n = 361.8 kg mol^{-1} and narrow dispersity $Đ$ = 1.25) was achieved.[33] However, it is difficult to completely remove tetrabutylammonium chloride from the polymer (tetrabutylammonium chloride can decompose and volatilize above 170 °C).[34] At such high temperatures, salicylate-based copolyesters (such as PSMG) tend to undergo a certain degree of degradation, which prevents the complete removal of tetrabutylammonium halides.[33]

In this work, DMF/DMSO was fortunately discovered as a green catalyst for the ROP of salicylate cyclic esters (Scheme 1). In this catalytic system, DMF/DMSO shows good selectivity toward the cleavage of the phenolic ester bond in the monomer rather than in polymer chains. Controllable high-molecular-weight copolyesters can also be achieved (PSMG with M_n =

[a]*State Key Laboratory of Natural Product Chemistry, College of Chemistry and Chemical Engineering, Lanzhou University, Lanzhou 730000, China. E-mail: wujc@lzu.edu.cn*

[b]*Baotou Research Institute of Rare Earths, China Northern Rare Earth (Group) High-tech Co., Ltd, Baotou 014030, People's Republic of China*

© 2025 The Author(s). Published by the Royal Society of Chemistry

Open Access Article. Published on 27 October 2025. Downloaded on 2/6/2026 11:08:24 AM.
This article is licensed under a Creative Commons Attribution-NonCommercial 3.0 Unported Licence.

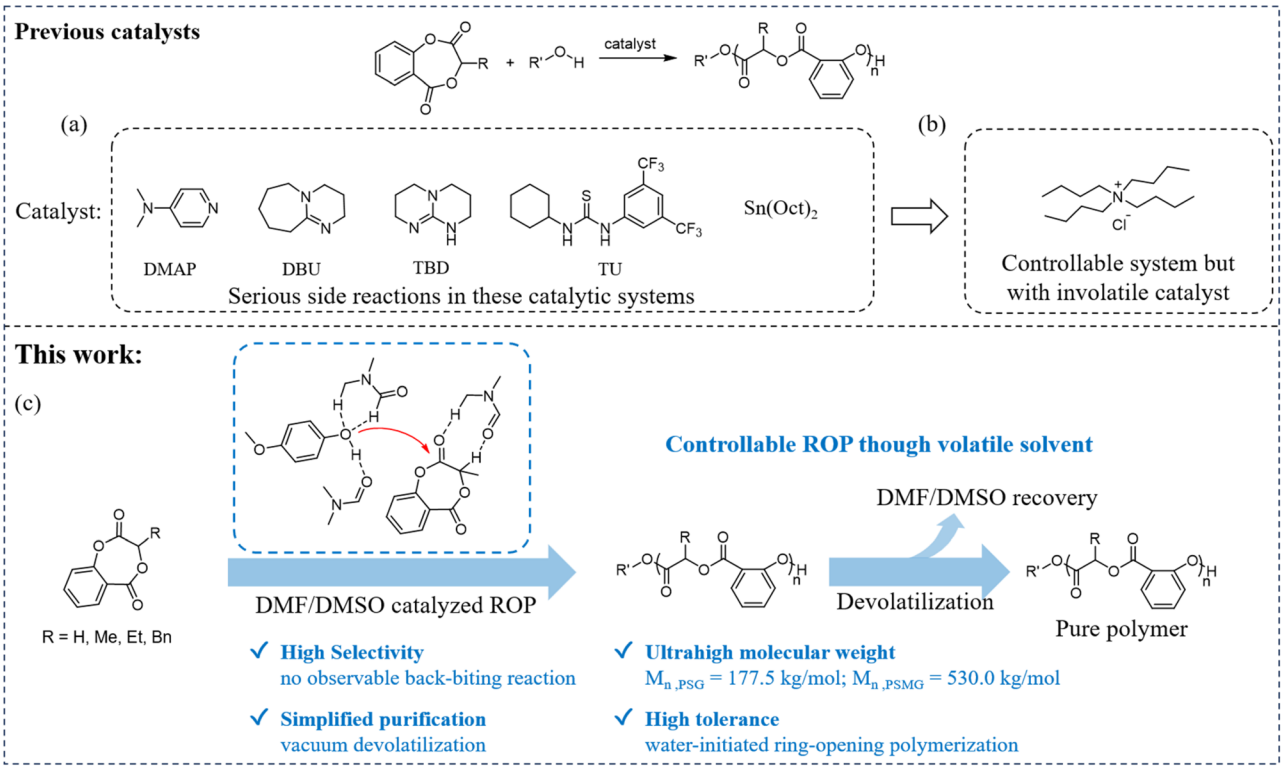

Scheme 1 (a) Previous catalysts for uncontrolled ROP of cyclic phenolic ester monomers. (b) TBACl for controlled ROP of cyclic phenolic ester monomers. (c) DMF/DMSO catalytic system for controlled ROP of cyclic phenolic ester monomers.

198 kg mol^{-1} and $Đ = 1.25$ using DMF and $M_n = 530.0$ kg mol^{-1} and $Đ = 1.28$ using DMSO). In addition, traces of water do not inhibit the controllability of the ROP of salicylate cyclic esters; replacing phenolic initiators with water still enables controlled ROP. More importantly, DMF/DMSO can be easily removed *via* a simple devolatilization process at room temperature. In this system, DMF/DMSO acts as both solvent and the catalyst and can be recycled through devolatilization under vacuum.

Results and discussion

Catalytic ROP of SMG, SEG, SG, and SBG using DMF/DMSO as solvent and catalytic species

Based on previous controllable ROP of salicylate cyclic esters catalyzed by tetrabutylammonium halides *via* hydrogen bond interactions between the catalyst, monomer, and initiator, the weak activation of the monomer is necessary to avoid activation of the phenolic ester bond in polymer chains and to selectively cleave the phenolic ester bond in the monomer rather than in polymer chains. After careful literature research, it was found that DMF[35,36] and DMSO[37–39] can act as weak Lewis bases to stabilize cationic intermediates and catalyze some organic reactions, for example, by raising intramolecular hydroarylation of alkene with simple arene,[35] by acting as Lewis base catalysts in the chlorination of (hetero)arenes,[38,39] and sometimes by playing a synergistic role with a base in the initiation of the radical process of α-arylation of enolizable aryl ketones.[36]

Thus, by employing DMF as both the solvent and catalyst, the ROP of lactic acid salicylate copolyester (PSMG) was conducted at 40 °C with *p*-methoxyphenol as the initiator, maintaining a ratio of $[I]_0/[PSMG]_0$ at 1 : 100 and a monomer concentration in DMF of 1 M. Under these conditions, 90% of the monomer was converted after 1 hour (Table S1, entry 2). Both the NMR molecular weight (Fig. S1) and the gel permeation chromatography molecular weight were consistent with the theoretical value of 18.0 kg mol^{-1}. When the temperature was decreased to 20 °C, the polymerization process became significantly slower (Table S1, entry 1), indicating that the energy barrier for this polymerization is not particularly low. Upon changing the solvent to a mixture of DMF and toluene, the polymerization was almost undetectable within 2.5 hours when the DMF content was below 20% (Table S2, entry 6). At a DMF proportion of 60 vol%, 56% of the monomer was converted under identical conditions, and the conversion gradually increased with higher DMF concentrations (Table S2, entries 1–5). All synthesized polymers exhibited M_n values that closely matched theoretical predictions and displayed narrow dispersity ($Đ$ = 1.2–1.3). However, the Size-Exclusion Chromatography (SEC) traces revealed shoulder peaks when 60–80 vol% DMF was used as the solvent (Fig. S2c–e), which disappeared when the DMF concentration reached ≥90 vol%, resulting in monomodal distributions (Fig. S2a and b). Therefore, DMF concentrations below 90 vol% not only reduced catalytic efficiency but also raised side reactions, likely due to insufficient activation of both the initiator and the monomer. Polymerization nearly ceased below 20 vol% DMF, further emphasizing the essential role of high DMF content in maintaining polymerization control.

© 2025 The Author(s). Published by the Royal Society of Chemistry

Open Access Article. Published on 27 October 2025. Downloaded on 2/6/2026 11:08:24 AM. This article is licensed under a Creative Commons Attribution-NonCommercial 3.0 Unported Licence.

Table 1 Controllable polymerization of SMG and SEG in DMF[a]

Entry	$[I]_0/[M]_0$	T/°C	t/h	Conv.[b]/%	$M_{n,calcd}$[c] (g mol^{-1})	$M_{n,NMR}$[c] (g mol^{-1})	$M_{n,obsd}$[d] (g mol^{-1})	$Đ$[d]
1	1 : 25	40	0.5	97	4700	6700	6300	1.16
2	1 : 100	40	1	90	18 000	25 900	22 000	1.28
3	1 : 200	40	2	97	38 300	47 000	50 000	1.31
4	1 : 400	40	2.5	99	76 000	80 000	83 000	1.25
5	1 : 600	40	3	99	115 000	—	128 000	1.23
6	1 : 800	40	3.5	99	153 000	—	155 000	1.29
7	1 : 1000	40	3.5	97	182 000	—	195 000	1.25
8[e]	1 : 500	40	3	96	99 000	—	115 000	1.18
9[e]	1 : 1000	40	4	98	202 000	—	217 000	1.31

[a] Conditions: under a dry N_2 atmosphere, DMF, initiator = *p*-methoxyphenol, $[M]_0$ = 1 M, monomer = SMG. [b] Determined using the ^{1}H NMR spectrum. [c] Calculated from $M_{SMG} \times [SMG]_0/[I]_0 \times$ conversion yield + $M_{p\text{-methoxyphenol}}$. [d] Absolute values of M_n and $Đ$ determined by SEC in THF. [e] SEG.

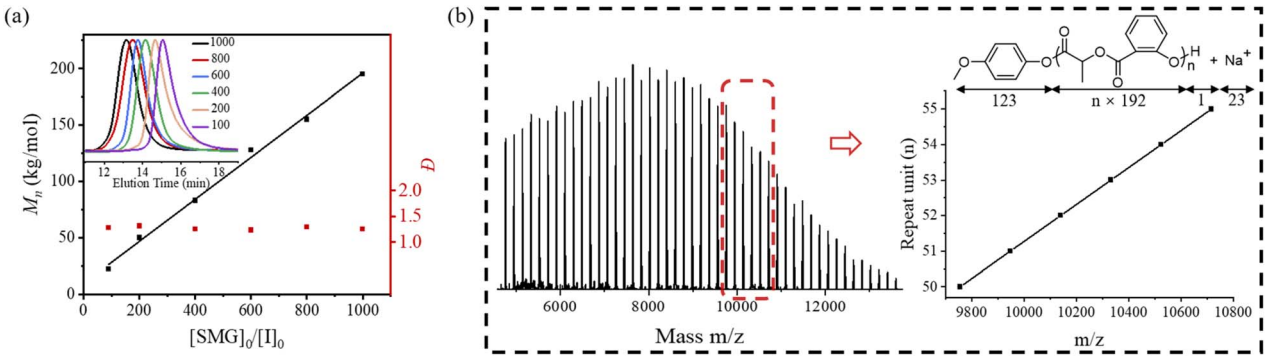

Fig. 1 (a) Plots of the relationship between M_n and molecular weight distribution $Đ$ of the polymer *versus* $[SMG]_0/[I]_0$ ratios, and representative SEC traces of PSMG (Table 1, entries 2–7); the black fitted line exhibits excellent correlation (R^2 = 0.99). (b) MALDI-TOF MS of PSMG was obtained in THF using DMF as a catalyst (Table 1, entry 1).

With the optimized catalytic system, the polymerization of the SMG monomer was systematically investigated at a constant monomer concentration ($[M]_0$ = 1 M) and varying $[I]_0/[M]_0$ ratios from 1 : 25 to 1 : 1000 (Table 1, entries 1–7). The experimental M_n values closely matched the theoretical predictions across the full $[SMG]_0/[I]_0$ range, exhibiting linear growth behavior (Fig. 1a). SEC analysis further confirmed narrow dispersity ($Đ \approx 1.25$) for all synthesized polymers, indicating controlled polymerization. Under optimal conditions ($[I]_0/[M]_0$ = 1 : 1000), PSMG with M_n = 198.0 kg mol^{-1} was successfully synthesized (Table 1, entry 7 and Fig. S11). After completion of the polymerization, direct solvent recovery was performed. Initial vacuum treatment at room temperature yielded a polymer with approximately 3% residual solvent, as determined by ^{1}H NMR analysis (Fig. S16). This corresponds to a solvent recovery efficiency of 97.8%. The polymer was heated to 130 °C under continued vacuum, after which no solvent signal was observed in the ^{1}H NMR spectrum (Fig. S17) to remove residual solvent. This method successfully enabled direct solvent recovery and efficient solvent removal. At an initial $[I]_0/[M]_0$ ratio of 1 : 25, matrix-assisted laser desorption/ionization time-of-flight mass spectrometry (MALDI-TOF MS) analysis of the resulting polymer (Table 1, entry 1) displayed a series of well-defined peak clusters at m/z = 123 + n × 192 + 1 + 23 (Fig. 1b), corresponding to polymer chains composed of n repeating SMG units ($\Delta m/z$ = 192 matching the monomer molecular weight). The terminated *p*-methoxyphenoxy end group, verified by both NMR and MALDI-TOF MS, confirmed the formation of linear polymers with controlled architecture. No cyclic polymers were detected in this MALDI-TOF MS, indicating that side reactions were minimal in this catalytic system. These findings indicated that DMF, serving as both solvent and the catalytic medium, can effectively and selectively activate phenolic ester groups in the monomer, enabling the controlled synthesis of high molecular weight polymers.

Methyl 2-((2-acetoxypropanoyl)oxy)benzoate (MAOB) was designed as a model compound representing the phenolic ester bond in polymer chains (Scheme S3, Fig. S3 and 4) to clarify the high selectivity of the DMF solvent system toward the cleavage of phenolic ester bonds in monomers rather than those within polymer chains. The chiral methine proton signal of MAOB at 5.37–5.41 ppm shifted to 5.22–5.26 ppm in the corresponding 4-methoxyphenyl-2-acetoxypropanoate (4-MAP) after the methyl salicylate group was substituted by the *p*-methoxyphenoxy group through a transesterification reaction between MAOB and *p*-methoxyphenol (Fig. 2 and S5–7). No reaction was observed between *p*-methoxyphenol and MAOB in DMF at 40 °C, even after 5 hours, as evidenced by the unchanged NMR

Open Access Article. Published on 27 October 2025. Downloaded on 2/6/2026 11:08:24 AM. This article is licensed under a Creative Commons Attribution-NonCommercial 3.0 Unported Licence.

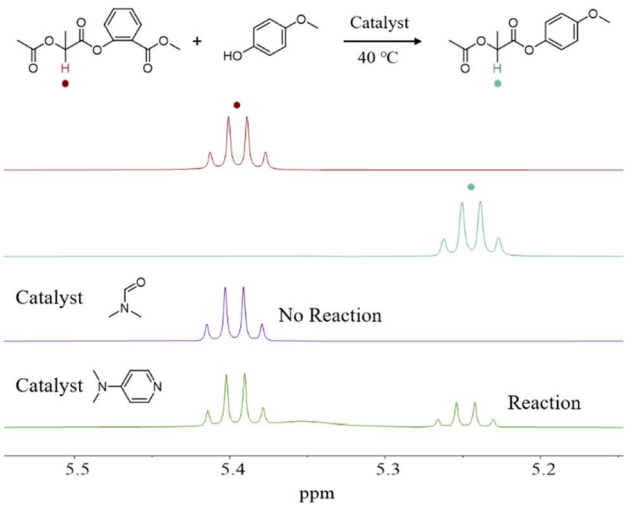

Fig. 2 Methine proton signals in ^{1}H NMR spectra for exploring the phenolic ester bond cleavage reaction of MAOB using DMF and DMAP as catalysts.

spectrum of MAOB. This result indicates that DMF cannot catalyze the cleavage of phenolic ester bonds in linear polymer chains. In contrast, under identical conditions with DMAP as a catalyst, 23% of MAOB was converted to 4-MAP, indicating a pronounced transesterification side reaction. These results demonstrate that high concentrations of DMF selectively activate phenolic ester bonds in cyclic SMG monomers while preserving those within polymer chains. This high selectivity ensures chain-end stability during propagation and is critical for synthesizing high molecular weight PSMG with narrow dispersity.

Then the ROP behaviors of other similar cyclic monomers, including salicylic glycolide (SG) (Scheme S1 and Fig. S8), salicylic ethyl glycolide (SEG) (Scheme S2 and Fig. S12), and salicylic benzyl glycolide (SBG) (Scheme S2 and Fig. S14), were systematically evaluated. Using DMF as a catalyst, the ROP of SEG exhibited good controllability. When the initiator-to-monomer ratio ($[I]_0/[M]_0$) varied from 1 : 500 to 1 : 1000 (Table 1, entries 8–9; Fig. S18a and b), the M_n values of poly(SEG) (PSEG) (Fig. S13) were consistent with theoretical predictions, achieving M_n = 217.0 kg mol^{-1} under 1 : 1000 conditions with narrow dispersity ($Đ$ = 1.31). However, experimental observations revealed that the DMF/p-methoxyphenol initiating system failed to promote the ROP of SG (Table S3, entry 1). When DMF was replaced with DMSO, due to its higher catalytic activity, SG polymerization proceeded effectively at $[I]_0/[M]_0$ = 1 : 25 (Table 2, entry 1). DFT calculations (Fig. S40) showed that the transition state of the SG monomer in DMF ($\mathbf{TS_{path6}}$) is approximately 2 kcal mol^{-1} higher than that in DMSO ($\mathbf{TS_{path7}}$). Therefore, the lower energy barrier in DMSO facilitates more efficient ring-opening polymerization of SG. The carbonyl carbon in $\mathbf{TS_{path7}}$ of the DMSO system carries a charge of +0.697, which is higher than that in $\mathbf{TS_{path6}}$ of the DMF system (+0.681), indicating that the phenolic ester bond of SG is more activated in DMSO than in DMF. In addition, with DMSO as a solvent, PSG maintained homogeneous dissolution throughout the ROP process, which represents a significant advancement considering its insolubility in THF/toluene. Systematic evaluation of the polymerization with $[M]_0/[I]_0$ ratios ranging from 1 : 25 to 1 : 1000 in DMSO ($[M]_0$ = 1 M, Table 2, entries 1–4) revealed linear molecular weight growth and narrow dispersity ($Đ$ < 1.24). With $[I]_0/[M]_0$ at 1 : 1000 (Table 2, entry 4 and Fig. S18c), the M_n of PSG (Fig. S9) achieved a record value of 177.5 kg mol^{-1}, surpassing literature-reported values.[32] Therefore, DMSO promotes polymerization due to its dual functionality as both a catalytic species and a solubilizing agent. Unlike SG, SMG, and SEG, the solubility of the SBG monomer in DMF is very low (monomer-insoluble/polymer-soluble), leading to anomalous SEC profiles (shoulder peaks, Table S3, entries 2 and 3, Fig. S19a and b) in the DMF catalytic system, possibly due to localized concentration gradients. In contrast, DMSO effectively resolved the solubility limitations of SBG (Table 2, entries 5 and 6), enabling the controlled synthesis of poly(SBG) (PSBG) (Fig. S15) with an M_n of up to 286.0 kg mol^{-1} ($Đ$ = 1.33) (Table 2, entry 6 and Fig. S18d). Under optimized conditions ($[I]_0/[M]_0$ = 1 : 2000) in the DMSO solvent catalytic system, the molecular weight of PSMG reached a high value of 530.0 kg mol^{-1} ($Đ$ = 1.31) (Table 2, entry 8; Fig. S18f). However, the observed $M_{n,obs}$ significantly exceeded the theoretical predictions for PSMG (Table 2, entries 7 and 8), which can be attributed to the high ring strain of the SMG monomer, endowing it with exceptionally high polymerization activity and enabling rapid chain propagation within a short

Table 2 Controllable polymerization of SG, SBG, SMG and SEG in DMSO[a]

Entry	$[I]_0/[M]_0$	T/°C	t/h	Conv.[b]/%	$M_{n,calcd}$[c] (g mol^{-1})	$M_{n,NMR}$[c] (g mol^{-1})	$M_{n,obsd}$[d] (g mol^{-1})	$Đ$[d]
1	1 : 25	40	0.5	95	4200	4500	4250	1.05
2	1 : 100	40	1	97	17 200	19 000	17 500	1.11
3	1 : 500	40	3	97	86 000	105 000	93 000	1.15
4	1 : 1000	40	5	99	176 220	—	177 500	1.24
5[e]	1 : 500	40	1	94	125 000	—	121 000	1.20
6[e]	1 : 1000	40	1.5	98	263 000	—	286 000	1.33
7[f]	1 : 1000	40	1	93	178 000	—	371 000	1.25
8[f]	1 : 2000	40	4	75	288 000	—	530 000	1.28
9[g]	1 : 1000	40	1.5	98	202 000	—	288 000	1.30

[a] Conditions: under a dry N_2 atmosphere, DMSO, initiator = p-methoxyphenol, $[M]_0$ = 1 M, monomer = SG. [b] Determined using the ^{1}H NMR spectrum. [c] Calculated from $M_{SMG} \times [SG]_0/[I]_0 \times$ conversion yield + $M_{p\text{-methoxyphenol}}$. [d] Absolute values of M_n and $Đ$ determined by SEC in mixed solvent $CHCl_3$ +30% HFIP (SG) and in THF (SBG, SMG, and SEG). [e] SBG. [f] SMG. [g] SEG.

© 2025 The Author(s). Published by the Royal Society of Chemistry

Open Access Article. Published on 27 October 2025. Downloaded on 2/6/2026 11:08:24 AM. This article is licensed under a Creative Commons Attribution-NonCommercial 3.0 Unported Licence.

timeframe. In addition, the dense solvation shell formed by highly polar DMSO molecules around the initiator could have caused the initiation rate to be slower than the propagation rate during ROP of SMG. Hence, the dependence of M_n on conversion was analyzed. Table S4 and Fig. S20 indicate that at low monomer conversion, the polymers exhibited relatively broad dispersities ranging from 1.7 to 1.9 (Table S4, entries 1 and 2, Fig. S21a and b). As conversion increased, dispersity gradually decreased to approximately 1.19 (Table S4, entry 4 and Fig. S21d). This observation indicates that during the early stage of polymerization, the initiator efficiency was relatively low, preventing complete initiation within a short time, while the high monomer reactivity led to rapid chain growth. Therefore, broad dispersity appeared in the SEC traces. As polymerization progressed and monomer conversion increased, the polymer chains reached higher molecular weights, and the non-uniform initiation in the early stage was masked by rapid chain growth and the formation of high molecular weight species, leading to narrow dispersity in the SEC traces. This set of experiments further confirmed that in DMSO, the initiator efficiency was suppressed, whereas high monomer reactivity drives rapid polymer chain growth, resulting in $M_{n,obsd}$ values deviating from $M_{n,calcd}$ values.

Melt polymerization represents a scalable production technology consistent with the principles of green chemistry and holds considerable industrial importance. DMSO was utilized to construct a solvation environment suitable for high-temperature reactions due to its high boiling point (189 °C) and low volatility to evaluate the applicability of solvent-catalyzed systems in melt polymerization. Controlled polymerization of SMG was achieved at an initiator-to-solvent ratio ($[I]_0/[DMSO]_0$) of 1 : 140 and $[I]_0/[M]_0 = 1:1000$ (a high monomer concentration $[M]_0 = 80$ M), producing PSMG with $M_n = 101.0$ kg mol^{-1} and $Đ = 1.14$ (Table S5, entry 9). These findings confirm that even under molten-state high-temperature conditions, DMSO effectively stabilizes active species through its solvation effects, suppressing side reactions.

Mechanistic studies

The interaction between DMF and the *p*-methoxyphenol initiator was examined using ^{1}H NMR titration in chloroform-d ($CDCl_3$) (Fig. 3a and Table S6) to gain further insight into the polymerization mechanism. The hydroxyl proton signal of *p*-methoxyphenol appeared as a single resonance, which exhibited significant downfield shifts upon incremental DMF addition (0.20–16.45 eq.). These shifts indicate dynamic hydrogen bonding between the phenolic OH and DMF, accompanied by rapid proton exchange on the ^{1}H NMR timescale. Job plot[40,41] analysis revealed a maximum change at a mole fraction value of approximately 0.34 (Fig. 3b), corresponding to a 1 : 2 binding stoichiometry between *p*-methoxyphenol and DMF. This observation demonstrates that two DMF molecules simultaneously coordinate with the initiator. Previous studies have shown that phenolic hydroxyl groups exhibit enhanced acidity in polar aprotic solvents.[42–44] In such systems, solvent molecules form a solvation shell around the polarized hydroxyl group of *p*-methoxyphenol through hydrogen bonding interactions, attenuating the coulombic interaction between the oxygen and proton while stabilizing the ionized state (schematic structural representation in Fig. 3b). In the present case, dynamic coordination with DMF compensates for entropic penalties through a synergistic effect, necessitating excess DMF (≥10.37 eq.) for full initiator activation. This cooperative solvation mechanism accounts for the requirement of high DMF concentrations to ensure effective initiator activation, overcoming the weak hydrogen-bonding ability of individual DMF molecules and enhancing their collective catalytic performance. This mechanism closely parallels that observed in recent studies on hexafluoroisopropanol (HFIP)-catalyzed cationic polymerization of vinyl monomers.[45] Similarly, ^{1}H NMR titration in $CDCl_3$ demonstrated that DMSO interacts with *p*-methoxyphenol in a manner analogous to that of DMF (Fig. S22 and Table S7). Job plot analysis revealed a maximum change at a mole fraction value of approximately 0.38 (Fig. S23), confirming a 1 : 2 binding stoichiometry between *p*-methoxyphenol and DMSO.

The ROP of SMG was conducted with four different DMF concentrations (100, 95, 90, and 85 vol% DMF in toluene), corresponding to 12.9, 12.3, 11.7, and 11.0 M, respectively, while maintaining a DMF volume fraction >80 vol% to suppress side reactions to determine the kinetic order of DMF in the catalytic system. Real-time monitoring of the polymerization (Fig. 3c) enabled determination of apparent rate constants (k_{app}) through first-order kinetic fitting on the monomer. Linear regression of $-\ln(k_{app})$ *versus* $-\ln([DMF]_0)$ yielded a slope of 3.35 ($R^2 = 0.99$; Fig. 3d), indicating a third-order dependence on the DMF concentration. Together with the previously established 1 : 2 solvent–initiator binding stoichiometry, these results support a trimolecular cooperative activation model in which the third DMF molecule likely interacts with the monomer *via* a hydrogen-bonding interaction (see DFT calculations, *vide infra*).

Fourier-transform infrared spectroscopy (FT-IR) was employed to probe dynamic interactions between DMF and the *p*-methoxyphenol initiator (Fig. S24) to substantiate the proposed mechanism. A gradient concentration protocol was applied. The O–H stretching vibration of *p*-methoxyphenol at 3367.53 cm^{-1} exhibited a pronounced red shift when the equivalents of DMF to *p*-methoxyphenol increased to 10.37 ($\Delta\nu \approx -120$ cm^{-1}, Fig. S24b). Simultaneously, the C=O stretching vibration of neat DMF at 1670.16 cm^{-1} displayed an initial red shift ($\Delta\nu \approx -8$ cm^{-1}) at low DMF equivalents to *p*-methoxyphenol (0.203 eq.; Fig. S24c), followed by a gradual return to the initial wavenumber (1670.16 cm^{-1}) as the DMF equivalents increased. Therefore, strong hydrogen bonding of O–H···O=C between the phenolic hydroxyl and the carbonyl group of DMF is evident. The C–O stretching vibration of *p*-methoxyphenol at 1231.06 cm^{-1} exhibited a distinct blue shift ($\Delta\nu \approx +4$ cm^{-1}, Fig. S24d), further indicating the DMF coordination effect. This shift plateaued between 1.83 and 2.74 DMF equivalents, corroborating the $[I]_0 : [DMF]_0 = 1:2$ stoichiometry determined by Job plot analysis through ^{1}H NMR titration. This spectral evolution reflects a dynamic coordination equilibrium, wherein excess DMF molecules offset entropic penalties through transient

Open Access Article. Published on 27 October 2025. Downloaded on 2/6/2026 11:08:24 AM.
This article is licensed under a Creative Commons Attribution-NonCommercial 3.0 Unported Licence.

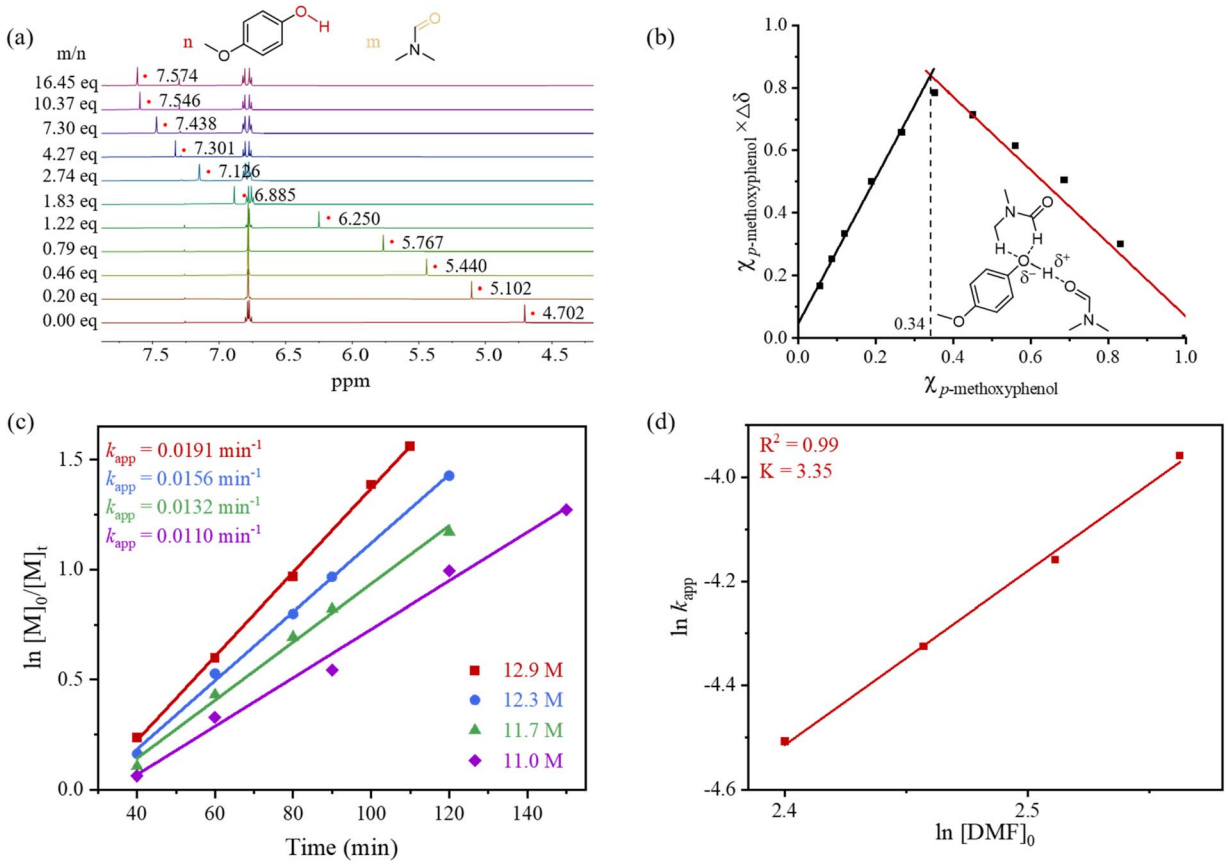

Fig. 3 (a) The binding interaction between DMF and the *p*-methoxyphenol was investigated *via* ^{1}H NMR titration in $CDCl_3$, monitoring proton signals of the hydroxyl group of *p*-methoxyphenol. (b) Job plot analysis for ^{1}H NMR titration (χ = [I]/([I] + [DMF]), $\Delta\delta = (\delta - \delta_0)$) and schematic structural representation of the 1 : 2 stoichiometric complex between *p*-methoxyphenol and DMF. (c) Plot of SMG conversion *vs.* time in four distinct DMF concentration systems. (d) Linear regression analysis of $-\ln(k_{app})$ *versus* $-\ln([DMF]_0)$.

interactions. Collectively, these findings demonstrate that DMF dynamically coordinates with *p*-methoxyphenol to enhance oxyanion electronegativity and nucleophilicity while maintaining rapid exchange.

However, the interaction between the SMG monomer and DMF at a DMF/SMG ratio ranging from 0.2 to 10 cannot be detected using FT-IR and ^{13}C NMR titration experiments, possibly because the interaction is very weak and the equilibrium constant is small for the complex formed between SMG and DMF. When large amounts of DMF were utilized, SMG became labile due to the ROP initiated by residual water (*vide infra*) with DMF acting as a catalyst. However, the third-order dependence on DMF indicates a potential interaction between SMG and DMF. Therefore, to clarify the catalytic role of DMF/DMSO in the ROP of the phenolic ester monomer, DFT calculations were conducted using methyl salicylate as a model initiator to simulate chain propagation conditions (Fig. 4). Initially, a trimolecular solvent-activation mechanism was proposed (Path 1 in Fig. 4a).

At the outset, two adducts were formed: $\mathbf{INT_{path1}}$ **1** (Fig. S29a), a complex consisting of two DMF molecules and one methyl salicylate molecule, and another complex composed of one DMF molecule and one SMG monomer. The catalytic mechanism proceeds through three coordinated steps: (1) initiator activation, one DMF molecule interacts with the initiator through pronounced hydrogen bonding (C=O···H–O); (2) oxygen anion stabilization, the second DMF molecule stabilizes the emerging oxyanion through weaker hydrogen bonds, enhancing ionization efficiency and electronegativity; and (3) monomer activation, the third DMF molecule polarizes the carbonyl group of SMG through hydrogen bonding, thus lowering the activation barrier for the ring-opening of the monomer. The transition state $\mathbf{TS_{path1}}$ (Fig. S29b) exhibited an activation barrier of 28.19 kcal mol^{-1}, which is dramatically lower than that of the solvent-free $\mathbf{TS_{path3}}$ (Fig. S25) barrier (42.26 kcal mol^{-1}). The Independent Gradient Model based on Hirshfeld partition (IGMH)[46–48] analysis revealed five characteristic hydrogen-bonding interactions (Fig. 4b and c). The synergistic effects of these interactions increased the electron density of the hydroxyl oxyanion, elevating its charge from −0.648e ($\mathbf{INT_{path1}}$ **1**) to −0.731e ($\mathbf{TS_{path1}}$). Simultaneously, monomer activation enhanced carbonyl polarization, increasing the ester carbon charge from +0.638e ($\mathbf{INT_{path1}}$ **1**) to +0.649e ($\mathbf{TS_{path1}}$). These findings confirm that DMF at a high concentration dynamically activates dormant species through weak non-covalent interactions. The trimolecular DMF coordination substantially reduces the activation energy barrier, facilitating efficient nucleophilic attack by the initiator on the

© 2025 The Author(s). Published by the Royal Society of Chemistry

Open Access Article. Published on 27 October 2025. Downloaded on 2/6/2026 11:08:24 AM.
This article is licensed under a Creative Commons Attribution-NonCommercial 3.0 Unported Licence.

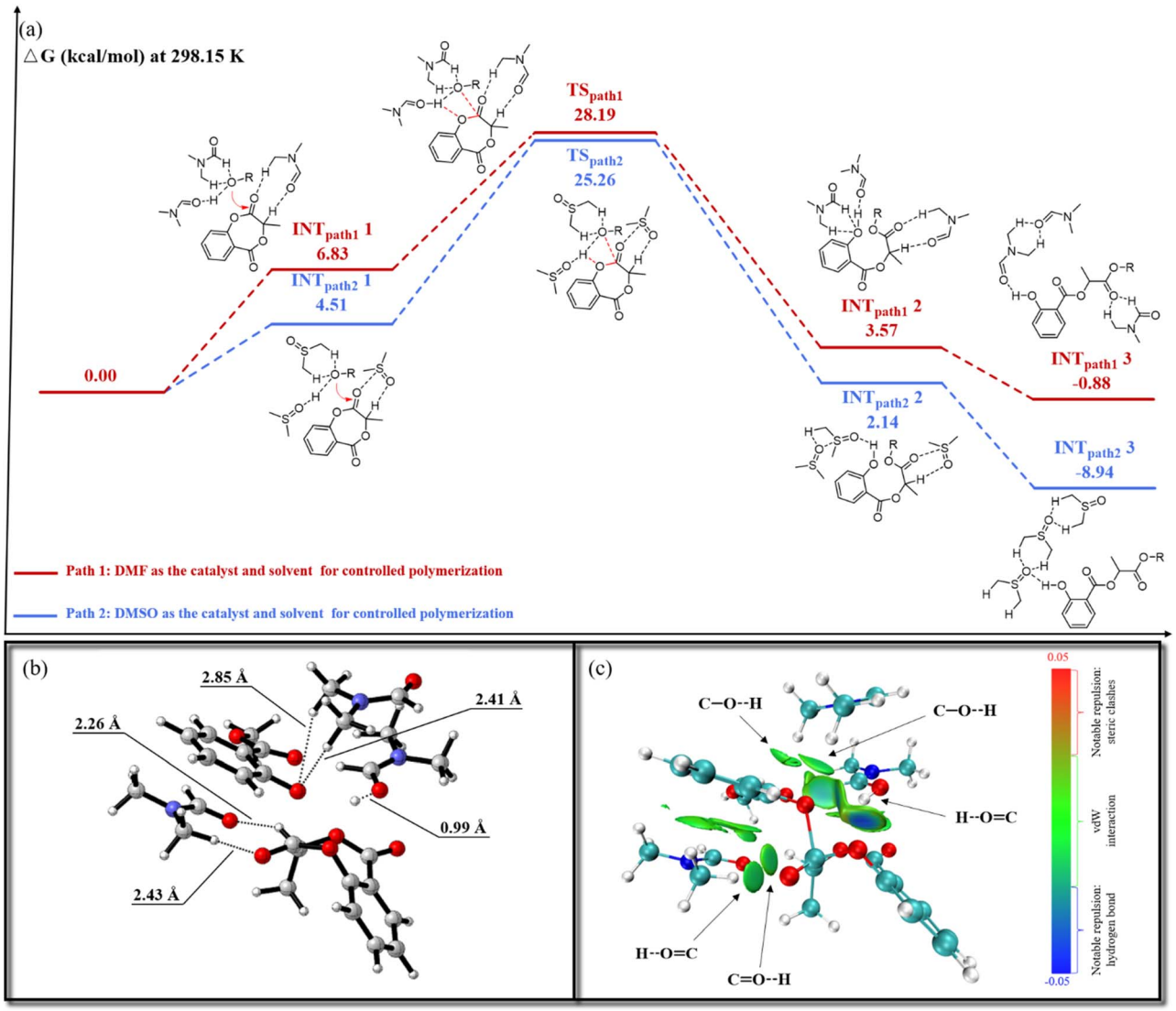

Fig. 4 (a) Gibbs free energy profile for the ROP of DMF/DMSO catalytic systems and mechanism for ROP of SMG. Calculations indicate a trimolecular solvent activation mechanism. (b) Optimized transition structure of TS_{path1}. (c) Local NCI analysis of TS_{path1} using IGMH method displaying the key five characteristic hydrogen-bonding interactions between methyl salicylate/SMG and DMF. Isosurfaces are generated for $s = 0.1$ a.u., and the colour scale is in the range of $0.05 < \rho < -0.05$ a.u. Dark blue, blue, green and red indicate regions of bond forming, notable attraction (hydrogen bond), van der Waals (vdW) interaction and notable repulsion (steric clashes), respectively.

SMG monomer. This process generates the active intermediate $\mathbf{INT_{path1}}$ **2** (Fig. S29c), which converts into the thermodynamically stabilized dormant species $\mathbf{INT_{path1}}$ **3** (Fig. S29d). The catalytic pathway involving two DMF molecules, without monomer activation, was also examined (Fig. S26); the energy barrier of $\mathbf{TS'_{path1}}$ at 35.71 kcal mol^{-1} was higher, indicating that during the catalytic process, the monomer is likely activated through the formation of a DMF-SMG adduct.

The catalytic ROP employing DMSO as both solvent and the catalyst was also analyzed (Fig. 4a, Path 2). Initially, the adducts $\mathbf{INT_{path2}}$ **1** (Fig. S31a) were formed through the coordination of two DMSO molecules with methyl salicylate and one DMSO molecule with SMG. The hydrogen bonding formation energy barrier between DMSO and methyl salicylate was calculated to be 4.51 kcal mol^{-1}, significantly lower than the 6.83 kcal mol^{-1} observed in the DMF system ($\mathbf{INT_{path1}}$ **1**), indicating stronger thermodynamic stabilization of the DMSO-initiator adduct. Then, the transition state $\mathbf{TS_{path2}}$ (Fig. S31b) exhibited an activation energy of 25.26 kcal mol^{-1}, which is 2.93 kcal mol^{-1} lower than that of $\mathbf{TS_{path1}}$ catalyzed by DMF. Similarly, for transition state $\mathbf{TS_{path2}}$ (Fig. S27a and b), non-covalent interaction (NCI)[49,50] analysis revealed four hydrogen bonds and a distinctive dipole–dipole interaction (2.87 Å). The sulfur atom in DMSO, bearing a substantial positive charge (+0.830e), enhanced dipole coupling with the carbonyl oxygen of the monomer. This interaction amplified carbonyl polarization, increasing the carbon charge to +0.701e, which is significantly higher than that in the DMF system (+0.649e). The reaction then proceeded to form the active intermediate $\mathbf{INT_{path2}}$ **2** (Fig. S31c), ultimately yielding the stabilized dormant species $\mathbf{INT_{path2}}$ **3**

Open Access Article. Published on 27 October 2025. Downloaded on 2/6/2026 11:08:24 AM. This article is licensed under a Creative Commons Attribution-NonCommercial 3.0 Unported Licence.

Table 3 Controllable water initiated ROP of SMG in DMF[a]

Entry	$[H_2O]_0/[M]_0$	T/°C	t/h	Conv. [b]%	$M_{n,calcd}$ [c] (g mol^{-1})	$M_{n,obsd}$ [d] (g mol^{-1})	$Đ$ [d]
1	1 : 200	40	2.5	91	34 900	41 000	1.43
2	1 : 400	40	3.5	93	71 400	59 000	1.24
3	1 : 600	40	3.5	90	103 000	83 000	1.21
4	1 : 800	40	4	94	145 000	111 000	1.16
5	1 : 1000	40	5	90	173 000	142 000	1.19

[a] Conditions: solvent = DMF, initiator = H_2O, $[M]_0$ = 1 M, monomer = SMG. [b] Determined using the ^{1}H NMR spectrum. [c] Calculated from $M_{SMG} \times [SMG]_0/[I]_0 \times$ conversion yield + $M_{p\text{-methoxyphenol}}$. [d] Absolute values of M_n and $Đ$ determined by SEC in THF.

(Fig. S31d). Collectively, the DFT calculations validated the trimolecular solvent-cooperative activation mechanism. Both pathways exhibited significantly lower activation barriers than the solvent-free condition ($\mathbf{TS_{path3}}$, 42.26 kcal mol^{-1}), highlighting the synergistic role of high-polarity aprotic solvents (DMF/DMSO) at elevated concentrations in activating phenolic initiators and cyclic ester monomers through multi-molecular coordination. The DMSO system demonstrated consistently lower barriers than DMF for both intermediates and transition states, signifying stronger intermolecular interactions among DMSO, the initiator, and the monomer. These enhanced interactions, particularly the robust dipole–dipole coordination, substantially improved the thermodynamic favorability of the ROP process.

Catalyst water tolerance experiment

Given the advantages of weak interactions in adapting to environmental conditions, the water tolerance of the catalytic system was systematically examined. Interestingly, this solvent catalytic system exhibited remarkable resistance to moisture. In DMF solvent under conditions of $[I]_0/[M]_0 = 1:600$, the addition of water at five equivalents (corresponding to 500 ppm in the solvent) relative to the initiator (Table S8, entry 4 and Fig. S33c) resulted in only a slight reduction in catalytic efficiency, with the monomer conversion decreasing by merely 16%. When water was considered an initiator, the experimental molecular weight closely matched the theoretical value. The SEC trace revealed a bimodal distribution ($Đ = 1.57$), indicating that water participated in the initiation process. However, the lower initiating efficiency of water compared to *p*-methoxyphenol likely caused the observed bimodality. Simultaneously, MALDI-TOF MS analysis (Fig. S34) revealed two distinct polymer populations initiated by *p*-methoxyphenol and water, respectively. At a lower water content of 100 ppm (Table S8, entry 2 and Fig. S33a), the SEC trace displayed a unimodal peak with a narrow dispersity ($Đ$ < 1.20), and the conversion exceeded 95%, indicating well-controlled polymerization. These results indicate that water-initiated ROP follows a slow initiation but a rapid propagation mechanism. In addition, DFT calculations revealed that employing water as an initiator (Fig. S36) yielded the transition state $\mathbf{TS_{path4}}$ (Fig. S37) with an activation barrier of 29.21 kcal mol^{-1}, slightly higher than that of $\mathbf{TS_{path1}}$ (28.19 kcal mol^{-1}). This finding validates the lower initiation efficiency of water relative to phenol initiators. Within the water initiation system, weak hydrogen bond interactions with DMF facilitated its activation as an initiator, promoting the ROP of monomers. This observation motivated further investigation of water as an initiator for the controlled ROP of phenolic ester monomers. At $[I]_0/[M]_0 = 1:200$ (Table 3, entry 1 and Fig. S33d), the experimental molecular weight closely approached the theoretical value, although the SEC trace exhibited a relatively broad distribution ($Đ = 1.43$), again reflecting the slow initiation and fast propagation nature of water in DMF. Increasing the feed ratio to $[I]_0/[M]_0 = 1:1000$ (Table 3, entry 5) significantly improved polymerization control, producing a polymer with a molecular weight of 142.0 kg mol^{-1} and a narrow dispersity ($Đ$ < 1.20). The molecular weight increased linearly with the monomer-to-initiator ratio, confirming the controllability of the solvent system. The presence of water did not disrupt the dynamic hydrogen bonding network in DMF. Instead, water molecules were activated by DMF through hydrogen bonding and directly participated in ROP. The strong moisture tolerance of the solvent system was further verified in DMSO. At $[I]_0/[M]_0 = 1:1000$, the addition of up to three equivalents of water (300 ppm) caused only a minor decrease in molecular weight (>300.0 kg mol^{-1}) without significantly affecting catalytic efficiency (Table S9, entries 2–4, Fig. S32g and h). Even at 500 ppm water (Table S9, entry 5 and Fig. S33i), the conversion decreased to 69%, but the polymerization remained well-controlled, yielding a high-molecular-weight polymer (282.0 kg mol^{-1}) with a narrow dispersity ($Đ = 1.16$). MALDI-TOF MS analysis detected polymer chains initiated solely by *p*-methoxyphenol, with no signals arising from water initiation (Fig. S35). DFT calculations demonstrated that the energy barrier for the process initiated by water was 3.22 kcal mol^{-1} higher ($\mathbf{TS_{path5}}$ = 28.48 kcal mol^{-1} *vs.* $\mathbf{TS_{path2}}$ = 25.26 kcal mol^{-1}, Fig. S38) than that for the reaction initiated by *p*-methoxyphenol in DMSO. Therefore, ROP initiated by water was suppressed by *p*-methoxyphenol. This DMF/DMSO solvent catalytic system exhibits outstanding water tolerance. Significantly, in DMF solvent, water can be effectively utilized as an initiator to achieve controlled ROP. This strategy not only addresses the challenge of catalyst residues but also eliminates initiator residue issues, greatly enhancing the biocompatibility and safety of the resulting polymers—an essential advantage for medical polymer development.

Conclusion

This study establishes a green and controllable polymerization system catalyzed by DMF and DMSO, enabling efficient ROP of cyclic phenolic ester monomers such as SG and SMG. In this

© 2025 The Author(s). Published by the Royal Society of Chemistry

Open Access Article. Published on 27 October 2025. Downloaded on 2/6/2026 11:08:24 AM. This article is licensed under a Creative Commons Attribution-NonCommercial 3.0 Unported Licence.

system, solvent molecules simultaneously act as both solvent and the catalyst, challenging conventional paradigms of catalyst design. Mechanistic investigations reveal a "solvent cooperative activation" mechanism: (1) the first solvent molecule activates the phenol initiator through a strong C═O···H–O hydrogen bond; (2) the second solvent molecule stabilizes the phenoxide anion intermediate *via* a weak C–H···O interaction; and (3) the third solvent molecule activates the ester bond in the monomer, reducing the nucleophilic attack barrier. The system demonstrates good moisture tolerance. Even in the presence of five equivalents of water relative to the initiator, effective polymerization control is maintained. Controlled ROP is successfully achieved using water as the initiator in DMF, yielding PSMG with a molecular weight of up to 142 kg mol^{-1} and a narrow dispersity ($Đ$ < 1.20). This approach fundamentally addresses the problems associated with catalyst and initiator residues, enhancing the biocompatibility and safety of the resulting polymers, simplifying post-processing, and reducing production costs. This solvent-catalyzed strategy presents a new perspective for ROP and broadens the application potential of bio-based phenolic ester polymers.

Author contributions

Jincai Wu supervised the project. Ge Yao carried out most of the experiments and wrote the initial manuscript draft. Jincai Wu and Ge Yao revised the manuscript. All authors discussed the results and commented on the manuscript.

Conflicts of interest

There are no conflicts to declare.

Data availability

Additional data supporting this article were provided in supplementary information (SI). Supplementary information: experimental details, the spectra of compouds and polymers, and theoretical calculation details. See DOI: https://doi.org/10.1039/d5sc06353a.

Acknowledgements

Financial support from the National Key R&D Program of China (2023YFA1506804) and the National Natural Science Foundation of China (nos. 22471110, 22131007, and 22171111) is gratefully acknowledged. We thank Dr Qingfeng Wu at the Institute of Modern Physics, Chinese Academy of Sciences for the MALDI-TOF mass measurement. We thank Prof. Shaoyu Lü and Dr Haofei Qie at the Lanzhou University College of Chemistry and Chemical Engineering for the FT-IR test.

Notes and references

1 *"Bioplastic market development update 2024"(European Bioplastics, 2024)*, European Bioplastics, https://www.european-bioplastics.org/bioplastics-market-development-update-2024/.

2 United Nations Environment Programme, *"Zero Draft of the plastics treaty (UNEP/PP/INC.3/4)" (UNEP, 2023)*, https://wedocs.unep.org/bitstream/handle/20.500.11822/43239/ZERODRAFT.pdf.

3 B. A. Abel and G. W. Coates, Introduction: The Future of Plastics Sustainability, *Chem. Rev.*, 2025, **125**, 1255–1256.

4 M. S. Kim, H. Chang, L. Zheng, Q. Yan, B. F. Pfleger, J. Klier, K. Nelson, E. L. W. Majumder and G. W. Huber, A Review of Biodegradable Plastics: Chemistry, Applications, Properties, and Future Research Needs, *Chem. Rev.*, 2023, **123**, 9915–9939.

5 X. L. Li, R. W. Clarke, H. Y. An, R. R. Gowda, J. Y. Jiang, T. Q. Xu and E. Y. X. Chen, Dual Recycling of Depolymerization Catalyst and Biodegradable Polyester that Markedly Outperforms Polyolefins, *Angew. Chem., Int. Ed.*, 2023, **62**, e202303791.

6 Z. Zhang, E. C. Quinn, J. L. Olmedo-Martinez, M. R. Caputo, K. A. Franklin, A. J. Muller and E. Y. Chen, Toughening Brittle Bio-P3HB with Synthetic P3HB of Engineered Stereomicrostructures, *Angew. Chem., Int. Ed.*, 2023, **62**, e202311264.

7 L. Zhou, Z. Zhang, C. Shi, M. Scoti, D. K. Barange, R. R. Gowda and E. Y.-X. Chen, Chemically circular, mechanically tough, and melt-processable polyhydroxyalkanoates, *Science*, 2023, **380**, 64–69.

8 Q. Cao, Y. M. Tu, H. Z. Fan, S. Y. Shan, Z. Cai and J. B. Zhu, Torsional Strain Enabled Ring-Opening Polymerization towards Axially Chiral Semiaromatic Polyesters with Chemical Recyclability, *Angew. Chem., Int. Ed.*, 2024, **63**, e202400196.

9 H. Z. Fan, X. Yang, J. H. Chen, Y. M. Tu, Z. Cai and J. B. Zhu, Advancing the Development of Recyclable Aromatic Polyesters by Functionalization and Stereocomplexation, *Angew. Chem., Int. Ed.*, 2022, **61**, e202117639.

10 C. Li, L. Wang, Q. Yan, F. Liu, Y. Shen and Z. Li, Rapid and Controlled Polymerization of Bio-sourced δ-Caprolactone toward Fully Recyclable Polyesters and Thermoplastic Elastomers, *Angew. Chem., Int. Ed.*, 2022, **61**, e202201407.

11 X. T. Wu, C. Yang, J. S. Xi, C. Shi, F. S. Du and Z. C. Li, Enabling Closed-Loop Circularity of "Non-Polymerizable" α, β-Conjugated Lactone Towards High-Performance Polyester with the Assistance of Cyclopentadiene, *Angew. Chem., Int. Ed.*, 2024, **63**, e202404179.

12 W. Zhao, Z. Guo, J. He and Y. Zhang, Solvent-Free Chemical Recycling of Polyesters and Polycarbonates by Magnesium-Based Lewis Acid Catalyst, *Angew. Chem., Int. Ed.*, 2025, **64**, e202420688.

13 J. Xian, H. Chen, G. Yao, F. Chen, Z. Chen, H. Cao, L. Cao, X. Pan, Y. Tang and J. Wu, Enantiomorphic Site-Assisted Chain End Control Stereospecific Alternating Copolymerization of Chiral Cyclic Diesters, *Angew. Chem., Int. Ed.*, 2025, **64**, e202420316.

14 A. Gadomska-Gajadhur and P. Ruśkowski, Biocompatible Catalysts for Lactide Polymerization—Catalyst Activity, Racemization Effect, and Optimization of the

Open Access Article. Published on 27 October 2025. Downloaded on 2/6/2026 11:08:24 AM. This article is licensed under a Creative Commons Attribution-NonCommercial 3.0 Unported Licence.

Polymerization Based On Design of Experiments, *Org. Process Res. Dev.*, 2020, **24**, 1435–1442.
15 S. C. Yoon, S. Y. Park, D. Y. Sim and I. S. Lee, Polylactide Resin Compositions with Good Mechanical Properties and Heat Resistance, *US Pat.*, 20120289675A1, 2012.
16 X. Geng, X. Liu, Q. Yu, C. Zhang and X. Zhang, Advancing H-Bonding Organocatalysis for Ring-Opening Polymerization: Intramolecular Activation of Initiator/Chain End, *J. Am. Chem. Soc.*, 2024, **146**, 25852–25859.
17 M. S. Young, A. M. LaPointe, S. N. MacMillan and G. W. Coates, Highly Enantioselective Polymerization of β-Butyrolactone by a Bimetallic Magnesium Catalyst: An Interdependent Relationship Between Favored and Unfavored Enantiomers, *J. Am. Chem. Soc.*, 2024, **146**, 18032–18040.
18 R. Morodo, D. M. Dumas, J. Zhang, K. H. Lui, P. J. Hurst, R. Bosio, L. M. Campos, N. H. Park, R. M. Waymouth and J. L. Hedrick, Ring-Opening Polymerization of Cyclic Esters and Carbonates with (Thio)urea/Cyclopropenimine Organocatalytic Systems, *ACS Macro Lett.*, 2024, **13**, 181–188.
19 Y. Xia, P. Yuan, Y. Zhang, Y. Sun and M. Hong, Converting Non-strained γ-Valerolactone and Derivatives into Sustainable Polythioesters via Isomerization-driven Cationic Ring-Opening Polymerization of Thionolactone Intermediate, *Angew. Chem., Int. Ed.*, 2023, **62**, e202217812.
20 J. Zhang, K. H. Lui, R. Zunino, Y. Jia, R. Morodo, N. Warlin, J. L. Hedrick, G. Talarico and R. M. Waymouth, Highly Selective O-Phenylene Bisurea Catalysts for ROP: Stabilization of Oxyanion Transition State by a Semiflexible Hydrogen Bond Pocket, *J. Am. Chem. Soc.*, 2024, **146**, 22295–22305.
21 J.-B. Zhu and E. Y. X. Chen, From meso-Lactide to Isotactic Polylactide: Epimerization by B/N Lewis Pairs and Kinetic Resolution by Organic Catalysts, *J. Am. Chem. Soc.*, 2015, **137**, 12506–12509.
22 A. Sanchez-Sanchez, I. Rivilla, M. Agirre, A. Basterretxea, A. Etxeberria, A. Veloso, H. Sardon, D. Mecerreyes and F. P. Cossío, Enantioselective Ring-Opening Polymerization of rac-Lactide Dictated by Densely Substituted Amino Acids, *J. Am. Chem. Soc.*, 2017, **139**, 4805–4814.
23 P. Lu, V. K. Kensy, R. L. Tritt, D. T. Seidenkranz and A. J. Boydston, Metal-Free Ring-Opening Metathesis Polymerization: From Concept to Creation, *Acc. Chem. Res.*, 2020, **53**, 2325–2335.
24 H.-Y. Huang, W. Xiong, Y.-T. Huang, K. Li, Z. Cai and J.-B. Zhu, Spiro-salen catalysts enable the chemical synthesis of stereoregular polyhydroxyalkanoates, *Nat. Catal.*, 2023, **6**, 720–728.
25 R. Xie, Y. Y. Zhang, G. W. Yang, X. F. Zhu, B. Li and G. P. Wu, Record Productivity and Unprecedented Molecular Weight for Ring-Opening Copolymerization of Epoxides and Cyclic Anhydrides Enabled by Organoboron Catalysts, *Angew. Chem., Int. Ed.*, 2021, **60**, 19253–19261.
26 C. K. Xu, G. W. Yang, C. Lu and G. P. Wu, A Binary Silicon-Centered Organoboron Catalyst with Superior Performance to That of Its Bifunctional Analogue, *Angew. Chem., Int. Ed.*, 2023, **62**, e202312376.
27 Q. Yan, J. Ma, W. Pei, Y. Zhang, R. Zhong, S. Liu, Y. Shen and Z. Li, Chemoselective Ring-Opening Polymerization of α-Methylene-δ-valerolactone Catalyzed by a Simple Organoaluminum Complex to Prepare Closed-Loop Recyclable Functional Polyester, *Angew. Chem., Int. Ed.*, 2024, **64**, e202418488.
28 Y. Zhu and Y. Tao, Stereoselective Ring-opening Polymerization of S-Carboxyanhydrides Using Salen Aluminum Catalysts: A Route to High-Isotactic Functionalized Polythioesters, *Angew. Chem., Int. Ed.*, 2024, **63**, e202317305.
29 A.-C. Albertsson and M. Hakkarainen, Designed to degrade, *Science*, 2017, **358**(6365), 872–873.
30 H. J. Kim, M. A. Hillmyer and C. J. Ellison, Enhanced Polyester Degradation through Transesterification with Salicylates, *J. Am. Chem. Soc.*, 2021, **143**, 15784–15790.
31 P. Salas-Ambrosio, S. Vexler, R. P Sivasankaran, N. Vlahakis, R. S. Lai, C. Johnson, S. I. Baas-Maynard, D. S. Min, H. Lower, A. G. Doyle, Y. Tang, J. A. Rodriguez, I. A. Chen, J. Read de Alaniz and H. D. Maynard, Biosourced Functional Hydroxybenzoate-co-Lactide Polymers with Antimicrobial Activity, *J. Am. Chem. Soc.*, 2025, **147**, 19230–19238.
32 H. J. Kim, Y. Reddi, C. J. Cramer, M. A. Hillmyer and C. J. Ellison, Readily Degradable Aromatic Polyesters from Salicylic Acid, *ACS Macro Lett.*, 2020, **9**, 96–102.
33 F. Ren, J. Xian, Z. Jia, Z. Chen, H. Fu, R. Wang, W. D. Chu, X. Pan and J. Wu, Tetrabutylammonium Halides as Selectively Bifunctional Catalysts Enabling the Syntheses of Recyclable High Molecular Weight Salicylic Acid-Based Copolyesters, *Angew. Chem., Int. Ed.*, 2023, **62**, e202306759.
34 W. Dołębska and T. Jaroń, Structural and thermal study of solvent-free tetrabutylammonium chloride and its novel solvates, *J. Mol. Struct.*, 2020, **1206**, 127748.
35 K. Lu, X.-W. Han, W.-W. Yao, Y.-X. Luan, Y.-X. Wang, H. Chen, X.-T. Xu, K. Zhang and M. Ye, DMF-Promoted Redox-Neutral Ni-Catalyzed Intramolecular Hydroarylation of Alkene with Simple Arene, *ACS Catal.*, 2018, **8**, 3913–3917.
36 M. Pichette Drapeau, I. Fabre, L. Grimaud, I. Ciofini, T. Ollevier and M. Taillefer, Transition-Metal-Free α-Arylation of Enolizable Aryl Ketones and Mechanistic Evidence for a Radical Process, *Angew. Chem., Int. Ed.*, 2015, **54**, 10587–10591.
37 Y. Ashikari, A. Shimizu, T. Nokami and J.-I. Yoshida, Halogen and Chalcogen Cation Pools Stabilized by DMSO. Versatile Reagents for Alkene Difunctionalization, *J. Am. Chem. Soc.*, 2013, **135**, 16070–16073.
38 S. Song, X. Li, J. Wei, W. Wang, Y. Zhang, L. Ai, Y. Zhu, X. Shi, X. Zhang and N. Jiao, DMSO-catalysed late-stage chlorination of (hetero)arenes, *Nat. Catal.*, 2019, **3**, 107–115.
39 H.-Q. Yue, D.-W. Shi, P. Zhang, B. Xiao, L.-T. Jia, R. Li, S.-N. Zhao, S.-D. Yang and B. Yang, DMSO-Catalyzed Double P–O Bond or Double P–S Bond Formations of Phosphinic Acids, *Org. Lett.*, 2024, **26**, 8939–8944.
40 J. S. Renny, L. L. Tomasevich, E. H. Tallmadge and D. B. Collum, Method of continuous variations: applications of job plots to the study of molecular

© 2025 The Author(s). Published by the Royal Society of Chemistry

Open Access Article. Published on 27 October 2025. Downloaded on 2/6/2026 11:08:24 AM.
This article is licensed under a Creative Commons Attribution-NonCommercial 3.0 Unported Licence.

associations in organometallic chemistry, *Angew. Chem., Int. Ed.*, 2013, **52**, 11998–12013.

41 W. Fang, Y. D. Meng, S. Y. Ding, J. Y. Wang, Z. H. Pei, M. L. Shen, C. Z. Yao, Q. Li, Z. Gu, J. Yu and H. J. Jiang, Asymmetric S-Arylation of Sulfenamides to Access Axially Chiral Sulfilimines Enabled by Anionic Stereogenic-at-Cobalt(III) Complexes, *Angew. Chem., Int. Ed.*, 2025, **64**, e202419596.

42 Z. Pawelka and T. Zeegers-Huyskens, Mid- and near-infrared study of hydrogen bond complexes between phenols and N,N-dimethylformamide, *Vib. Spectrosc.*, 1998, **18**, 41–49.

43 M. G. Siskos, V. G. Kontogianni, C. G. Tsiafoulis, A. G. Tzakos and I. P. Gerothanassis, Investigation of solute–solvent interactions in phenol compounds: accurate ab initio calculations of solvent effects on 1H NMR chemical shifts, *Org. Biomol. Chem.*, 2013, **11**, 7400–7411.

44 F. G. Bordwell, R. J. McCallum and W. N. Olmstead, Acidities and Hydrogen Bonding of Phenols in Dimethyl Sulfoxide, *J. Org. Chem.*, 1984, **49**, 1424–1427.

45 M. Li, X. Ma and Y. Tao, Unlocking Hexafluoroisopropanol as a Practical Anion-Binding Catalyst for Living Cationic Polymerization, *Angew. Chem., Int. Ed.*, 2025, **64**, e202425178.

46 T. Lu and Q. Chen, Independent gradient model based on Hirshfeld partition: A new method for visual study of interactions in chemical systems, *J. Comput. Chem.*, 2022, **43**, 539–555.

47 T. Lu and F. Chen, Multiwfn: a multifunctional wavefunction analyzer, *J. Comput. Chem.*, 2012, **33**, 580–592.

48 T. Lu, A comprehensive electron wavefunction analysis toolbox for chemists, Multiwfn, *J. Chem. Phys.*, 2024, **161**, 082503.

49 E. R. Johnson, S. Keinan, P. Mori-Sánchez, J. Contreras-García, A. J. Cohen and W. Yang, Revealing Noncovalent Interactions, *J. Am. Chem. Soc.*, 2010, **132**, 6498–6506.

50 W. Humphrey, A. Dalke and K. Schulten, VMD: Visual molecular dynamics, *J. Mol. Graph.*, 1996, **14**, 33–38.